Published in final edited form as:
Retina. 2006 ; 26(6): 655–660.

QUANTIFICATION OF PHOTORECEPTOR LAYER THICKNESS IN NORMAL EYES USING OPTICAL COHERENCE TOMOGRAPHY

Annie Chan, MD[*], **Jay S. Duker, MD**[*], **Hiroshi Ishikawa, MD**[†], **Tony H. Ko, PhD**[‡], **Joel S. Schuman, MD**[†], and **James G. Fujimoto, PhD**[‡]

*****New England Eye Center, Tufts-New England Medical Center, Tufts University School of Medicine, Boston, Massachusetts

†University of Pittsburgh Medical Center Eye Center, Department of Ophthalmology, University of Pittsburgh School of Medicine, Pittsburgh, Pennsylvania

‡Department of Electrical Engineering and Computer Science, Research Laboratory of Electronics, Massachusetts Institute of Technology, Cambridge, Massachusetts.

Abstract

Objective—To demonstrate the ability to segment and analyze individual intraretinal layers, including the outer retinal complex (ORC; outer nuclear layer and inner and outer segments of the photoreceptor cells), in healthy eyes using images acquired from the latest commercially available optical coherence tomography (OCT) system (StratusOCT; Carl Zeiss Meditec, Inc., Dublin, CA) and from the ultrahigh resolution OCT (UHR-OCT) prototype.

Methods—Thirty-seven eyes from 37 healthy subjects underwent complete ophthalmologic examination using StratusOCT and UHR-OCT. ORC was identified and measured using a segmentation algorithm.

Results—For StratusOCT, mean weighted ORC thickness ± SD was 91.1 ± 7.9 μm, and mean weighted total retinal thickness ± SD was determined to be 258.9 ± 10.1 μm. For UHR-OCT, mean weighted ORC thickness ± SD was 96.4 ± 6.3 μm, and mean weighted total retinal thickness ± SD was determined to be 263.4 ± 9.2 μm. There was a higher rate of algorithm failure with UHR-OCT images.

Conclusions—Photoreceptor layer thickness can be calculated by measuring ORC on OCT images using a macular segmentation algorithm. ORC values may serve as a useful objective parameter in determining the efficacy of various therapeutic modalities that target the photoreceptor layer in various diseases.

Keywords

optical coherence tomography; photoreceptor; retinal imaging

Optical coherence tomography (OCT) has emerged as an important imaging modality in the evaluation and management of retinal disease. The ability to noninvasively image intraocular structures in vivo with resolution approaching that of histologic analysis has made OCT particularly useful in the detection and quantification of macular edema.[1–6] OCT may also provide valuable quantitative information for retinal degenerative processes such as age-related related macular degeneration and the hereditary retinal dystrophies. In these conditions, selective outer retinal degeneration (photoreceptor cells) leads to visual loss. Nutritional

Reprint requests: Jay S. Duker, MD, Tufts-New England Medical Center, New England Eye Center, 750 Washington Street, Box 450, Boston, MA 02111-1533.

supplementation, administration of growth factors, gene therapy, retinal pigment epithelium transplantation, antiapoptotic treatment, and other strategies have been proposed to slow the progression of photoreceptor cell loss with varying degrees of success.[7,8] As these new promising therapies are studied in clinical trials, OCT may ay aid in evaluating the efficacy of these treatments by quantifying the photoreceptor receptor cell layer in a reliable and reproducible way.

The introduction of the currently available commercial OCT unit (StratusOCT, Carl Zeiss Meditec, Inc., Dublin, CA) represented a marked improvement in imaging speed (scanning speed, 100–400 Hz) with a standard 10-μm OCT axial resolution. Our group has developed an ultrahigh resolution OCT (UHR-OCT) prototype that is capable of achieving axial resolution of <3 μm.

The purpose of this study was to measure normal photoreceptor layer thickness in healthy eyes using a software algorithm designed to perform automated segmentation of retinal layer structures on images obtained by StratusOCT and UHR-OCT. The photoreceptor receptor layer represents a small mall fraction of overall macular thickness, and changes in the total macular thickness due to photoreceptor cell loss may be subtle. Segmentation of intraretinal layers would allow clinicians to quantify specific layers that are affected in certain diseases.

Methods

Approval for this study was obtained from the Human Investigation Review Committee at the Tufts-New England Medical Center (Boston, MA). All participants engaged in an informed consent process and signed a written consent document before study procedures were carried out. Healthy subjects were examined at the New England Eye Center between August 2003 and February 2004. All participants underwent complete ophthalmologic examination including medical and family history, best-corrected visual acuity testing with EDTRS charts, Humphrey Swedish Interactive Thresholding Algorithm Standard 24-2 perimetry (Carl Zeiss Meditec), applanation tonometry, slit-lamp biomicroscopy, indirect ophthalmoscopy, and color fundus photography. OCT was performed on a dilated pupil by an experienced operator using StratusOCT and UHR-OCT.

Exclusion criteria for normal eyes included any history or evidence of retinal disease; diabetes or other systemic disease that could affect the eye; glaucoma or a first-degree relative with glaucoma; intraocular pressure of >21 mmHg; abnormal visual fields; intraocular surgery or laser therapy, although refractive surgery >1 year before enrollment was acceptable; best-corrected visual acuity worse than 20/32; and refractive error greater than +6.00 diopters or less than −6.0 diopters.

OCT was performed within well established safe retinal exposure limits established by the ANSI standard. The ANSI standard for safe retinal exposure accounts for wavelength, duration, and multiple exposures of the same spot on the retina.

The StratusOCT images were generated using scans of 2-mm axial depth and 6 mm in the transverse direction. Each image had ≈10-μm axial and 20-μm transverse resolutions in tissue and consisted of 1,024 axial pixels and 512 transverse pixels (total, 524,288 pixels). StratusOCT uses a superluminescent diode light source that generates an ≈25-nm bandwidth centered at an 800-nm wavelength. The scanning rate is 400 A-scans per second, or ≈1.3 seconds per 512 A-scan image. The macular map scan protocol was used for both systems. Good quality images were defined as those with quality index values of >17.5. This value was found to be more sensitive than the conventional signal-to-noise ratio.[9] Images with a quality index value of <17.5 were considered poor in quality and were excluded. Quality index values

have not been established for UHR-OCT. Therefore, image quality for UHR-OCT was determined subjectively.

A prototype UHR-OCT system with a femtosecond titanium:sapphire laser as the OCT imaging light source was designed and developed for clinical use. The laser generated an ≈125-nm bandwidth centered at an 815-nm wavelength. The UHR-OCT images were generated using scans of 1.5-mm axial depth and 6 mm in the transverse direction. Each image had ≈3-μm axial and 15- to 20-μm transverse resolutions in tissue and consisted of 3,000 axial pixels and 600 transverse pixels (total, 1,800,000 pixels), ≈3 to 4 o times better resolution than the standard commercial StratusOCT systems. The scanning rate was slower, taking 4.3 seconds to acquire each image. UHR-OCT was performed using up to 750 μW of incident optical power in the OCT scanning beam. The UHR-OCT prototype system is based on a slit-lamp biomicroscope with an integrated charge-coupled device imager (CCD) to provide a video image of the fundus. The patient's eye position was established by using internal fixation targets. Once scanning was completed, both the StratusOCT and UHR-OCT images were corrected for axial motion using standard reregistration algorithms. These algorithms have been used in all previous prototype and commercial systems.[10]

An algorithm was developed using a software development environment (Visual Studio.Net, Microsoft, Redmond, WA). Raw OCT data files were exported to an IBM compatible personal computer. This algorithm searched for borders of retinal layer structures on each sampling line (analogous to the A-scan line of ultrasonography) by applying an adaptive thresholding technique. A set of normal macular OCT images (learning set) had been used to design the algorithm. The summarized flow of the algorithm was as follows. **Preprocessing:** 1. Aligned z-offset (starting location of the meaningful signal on each sampling line) by cross-correlation (shifting sampling lines so that the sum of the products of adjacent pixels is maximized). 2. Equalized the histogram of pixel intensity on each line by scaling the pixel intensities to the same minimum and maximum values. 3. Applied a modified mean filter (kernel size, 7 × 5) to remove speckles. **Segmentation:** 1. Sought the internal limiting membrane on each sampling line. The internal limiting membrane was defined as the first highly reflective rise from the inner side on each sampling line. Usually, it was well demarcated and easily detected. This rise should be followed by a sector of high reflectivity. If not, the rise could represent noise. The actual location of the border was determined using an adaptive thresholding technique, where a cutoff threshold value was calculated based on reflectivity characteristics of each sampling line. An integrity check with adjacent sampling lines was then performed to detect any disruption on the line of each of the detected structures by looking at the derivatives of the border location between the adjacent sampling lines. If the integrity check failed, the software automatically altered the internal parameters of the target peak (e.g., reflectivity threshold, peak width, peak height, etc) within a certain range and reran the seeking procedure. Another integrity check was then performed. If it failed, a quadratic regression line of the detected border locations was calculated in the vicinity of the target sampling line, and the closest eligible slope was determined to this regression line in the same fashion described above. The ability to discriminate noise from true tissue reflectivity was enhanced by this integrity check. 2. Sought the retinal pigment epithelium on each sampling line. The algorithm tried to detect two major peaks on each sampling line. The inner border of the second peak was then registered as the retinal pigment epithelium complex. A notch or gap close to this inner border within the complex was finally detected as the retinal pigment epithelium. The inner border was registered as the interface between inner and outer segments of the photoreceptor. A series of integrity checks and adjustment procedures described above were performed for each detected border line thereafter. The area between internal limiting membrane and photoreceptor interface was registered as the retinal complex. 3. The deepest and widest valley within the retinal complex was registered as the outer retinal complex (ORC), which consisted of the outer nuclear layer and the inner segment of the photoreceptor layer. 4. The inner most prominent peak between

the internal limiting membrane and the inner border of ORC was registered as macular nerve fiber layer. 5. The outer most peak before ORC was registered as the outer plexiform layer. 6. The residual area between the outer border of the macular nerve fiber layer and the inner border of the outer plexiform layer was finally registered as the inner retinal complex, which consisted of the retinal ganglion cell layer, inner plexiform layer, and inner nuclear layer. **Thickness Mapping Plotting:** 1. After calculating the thickness for each segment (macular nerve fiber layer, inner retinal complex, outer plexiform form layer, and ORC) on each image, the thickness values of a set of six radial linear macular scan images were plotted on a Cartesian plane. 2. Values for points in between actual measurements on the plane were calculated by polar interpolation.[11]

All linear macular OCT images were analyzed using the algorithm. Algorithm performance was subjectively evaluated by a human expert to detect algorithm errors. Criteria for algorithm error included the following: obvious disruption of the detected border, and/or border wandering (detected border jumping to and from different anatomical structures) for >15% (continuous) or 20% (cumulative) of the entire image. In the StratusOCT images, there are 512 sampling lines. Therefore, 77 continuous lines (15%) or 102 cumulative lines (20%) of disruption were considered failures. The layer of interest in this study was ORC. ORC is composed of the outer nuclear layer and the inner and outer segments of the photoreceptor cells. Because border detection reliability was low (high error rate) at the interface between inner and outer segments of the photoreceptor layer, the layers were combined to maximize measurement reliability. The thickness of the ORC segment was calculated for each linear macular image. For each patient, weighted mean ORC thickness was generated from all good quality images, representing an interpolated weighted average. If there were more than two individual images that failed the algorithm within a set of six images for each patient, the case was excluded. If there were at least two consecutive images (e.g., 60° and 90° radial scans) that failed the algorithm, the case was also excluded. The weighted ORC thickness values by StratusOCT and UHR-OCT were compared with paired *t*-tests. Statistical analysis was performed with SPSS 11.0.1 (SPSS, Inc., Chicago, IL). Furthermore, more, an analysis was performed on scans that had 100% successful border mapping with both StratusOCT and UHR-OCT. The results were compared with the entire data.

Results

Thirty-seven normal eyes from 37 healthy subjects were examined clinically and by both StratusOCT and UHR-OCT. The patients' ages ranged from 22 years to 71 years (median, 43 years). There were 26 women (70%) and 11 men (30%). One patient was excluded from the StratusOCT group due to algorithm error. UHR-OCT images were also evaluated by this algorithm. There was a higher rate of algorithm failure with UHR-OCT images. Six patients in this group were excluded due to algorithm error. Of the 31 remaining patients, only 11 had 100% successful border mapping with both StratusOCT and UHR-OCT.

Mean weighted ORC thickness ± SD was determined to be 91.1 ± 7.9 μm by StratusOCT versus 96.4 ± 6.3 μm by UHR-OCT. Mean weighted total retinal thickness ± SD was determined to be 258.9 ± 10.1 μm by StratusOCT versus 263.4 ± 9.2 μm b by UHR-OCT. Mean weighted ORC thickness ± SD measured by StratusOCT and UHR-OCT according to age (20–29 years [8 eyes], 30–39 years [4 eyes], 40–49 years [6 eyes], 50–59 years [9 eyes], and 60 years or older [4 eyes]) is shown in Figure 1 and Figure 2. Overall, the mean weighted ORC thickness ± SD was significantly lower by StratusOCT than by UHR-OCT (91.1 ± 7.9 μm vs. 96.4 ± 6.3 μm, respectively; $P = 0.002$ [paired *t*-test]).

Using linear regression analysis, ORC does not appear to change with age ($P = 0.54$ for StratusOCT and $P = 0.075$ for UHR-OCT).

For the 11 patients who had 100% successful border mapping with both StratusOCT and UHR-OCT, mean weighted ORC thickness ± SD was determined to be 90.9 ± 9.3 μm by StratusOCT versus 96.6 ± 4.7 μm by UHR-OCT. Mean weighted total retinal thickness ± SD was determined to be 262.1 ± 7.9 μm by StratusOCT versus 267.3 ± 8.4 μm by UHR-OCT.

Discussion

The present study demonstrates that a software algorithm designed to automatically segment and quantify intraretinal layers of clinical interest, such as the photoreceptor layer, on two-dimensional OCT images is feasible. Recently, Ishikawa et al [11] showed that this algorithm may be useful in discriminating between normal and glaucomatous eyes by objectively quantifying damage to the inner retinal complex (composed of the retinal ganglion cell layer, inner plexiform layer, and inner nuclear layer) and the nerve fiber layer.

Our study was performed with the understanding that the assignment of substructures within the photoreceptor layer is challenging. The identification of intraretinal layers is complicated by the fact that the macula can change drastically even after short periods of ischemia and can be further distorted by histologic processing. There are few histologic examples of normal primate and human foveae free of postmortem changes.[12] Findings of earlier studies attempting to measure the outer segments were inconsistent.[13,14] Huang et al [15] suggested that formalin and paraformaldehyde used as agents in earlier histologic studies were poor fixatives of the retina, especially the outer segment, and that fixation in glutaraldehyde and embedding in plastic would better preserve tissue. More recent work on monkey and human retinas using glutaraldehyde showed that the outer segment measured ≈20μm to 30μm in foveal thickness and was 20% of the total retinal thickness.[16] The results of these studies agree very well with the outer segment measurements from the UHR-OCT images. Since then, other studies have provided evidence to support good correlation between UHR-OCT and histologic analysis of pig retina.[12,17]

Physicians should be aware that correlation between OCT and histologic analysis may not be exact because OCT signals are directly determined by the optical properties of tissue. These signals are affected by the absorption, reflection, and scattering of light, as well as the orientation of the tissue components. As a result, components that stain strongly during histologic logic analysis may not correlate with intense OCT signals. For example, the reflective signal at the junction between inner and outer segments of the photoreceptor receptor cells is due to an abrupt change in the index of refraction. This change is probably caused by the highly organized structure of the stacks of membranous disk contained in the outer segments.[18] The highly organized outer segment is rich in the visual pigment rhodopsin and has a higher index of refraction than the less organized inner segment.

The values determined in our study are consistent with findings of a previous study by Hermann et al[19] in which photoreceptor layer thickness was determined mined by counting the number of pixels from the inner border of the outer nuclear layer to the outer border of the outer segments of the photoreceptor layer. Only a few patients were included in that study, and values were given only for the center of the fovea. These researchers found the mean photoreceptor layer thickness ness to be ≈90 μm at the center of the fovea.

In our study, UHR-OCT images had a higher rate of algorithm failure than StratusOCT images. This is most likely due to the inherent differences between StratusOCT and UHR-OCT, such as the characteristics of the speckle noise. The algorithm used in this study is optimized for StratusOCT images. In theory, UHR-OCT should produce fewer failures because of higher resolution. Further refinements in the algorithm will allow for more accurate measurements by both StratusOCT and UHR-OCT. In an attempt to separate algorithm failure from other

causes of variability, we analyzed a subset of 11 patients with 100% successful border mapping with both instruments. The SD for mean weighted total retinal thickness by StratusOCT and UHR-OCT, as well as for mean ORC thickness by UHR-OCT, decreased, but the SD for mean ORC thickness by StratusOCT increased. Because UHR-OCT had a higher rate of algorithm failure than StratusOCT in this study, it is not surprising that when algorithm failure was removed as a variable, the SDs decreased for the UHR-OCT measurements.

Some previous reports have speculated that retinal thickness or photoreceptor layer thickness decreases with age, but there was no evidence in this study to support that claim. Future studies with larger sample sizes and better representation of all age groups are needed. In this study, ORC thickness measurements by StratusOCT were significantly lower than those by UHR-OCT (Fig. 1). This may be due to better border detection as a result of higher image resolution of UHR OCT.

Several technical challenges remain for the physician in using OCT to diagnose and monitor disease progression. Given the inherent problems of saccadic movements, fixation losses, and differences in patient positioning between visits and between scans, it is indeed difficult to be certain that one is scanning the exact same macular region at each visit without reliable anatomical landmarks. Faster imaging speeds and thus more rapid acquisition of data may mitigate these problems.[10] Furthermore, the current scanning protocol used in the commercial OCT system of six radial lines converging at the center, with the interpolation of data points for generating a map of the retina, can be improved such that a higher density of cross-sectional sectional planes can be obtained. This would increase the sensitivity of detecting focal defects. Several experimental protocols are currently being developed and tested.

In the Western world, age-related macular degeneration is the main cause of visual loss in adults older than 65 years of age, while retinitis pigmentosa represents the most common cause of blindness in people younger than 70 years of age.[7] Selective outer retinal damage and loss of photoreceptors lead to loss of vision in both conditions. Currently, there is no cure for either condition, but intense research efforts are under way.

Some modest therapeutic responses, as judged by subjective improvement, have been made, but scientific validation of these claims is difficult. OCT may aid in evaluating the efficacy of these treatments by quantifying the photoreceptor cell layer in a reliable and reproducible way. It is possible to create segmented linear or three-dimensional maps composed of certain retinal layers of interest, such as ORC, from the original six linear macular images using the software ware in this study. This could greatly enhance our understanding of retinal disease.

Photoreceptor layer thickness can be calculated by measuring ORC with optical coherence tomography using a macular segmentation algorithm. ORC values may serve as a useful objective parameter in determining the efficacy of various therapeutic modalities that target the photoreceptor layer.

Acknowledgements

Supported in part by the National Institutes of Health National Eye Institute, Bethesda, MD (grants RO1-EY013178-5, R01-EY11289-19, and P30-EY008098); The Eye and Ear Foundation, Pittsburgh, PA; an unrestricted grant from Research to Prevent Blindness, Inc., New York, NY; the National Science Foundation, Arlington, VA (grant ECS-0119452); and the Medical Free Electron Laser Program, Air Force Office of Scientific Research, Arlington, VA (contract F49620-01-1- 0186). J.G.F. and J.S.S. receive royalties from intellectual property licensed by Massachusetts Institute of Technology (Cambridge, MA) to Carl Zeiss Meditec, Inc. (Dublin, CA).

References

1. Huang D, Swanson EA, Lin CP, et al. Optical coherence tomography. Science 1991;254:1178–1181. [PubMed: 1957169]

2. Swanson EA, Izatt JA, Hee MR, et al. In vivo retinal imaging by optical coherence tomography. Opt Lett 1993;18:1864–1866.

3. Hee MR, Izatt JA, Swanson JA, et al. Optical coherence tomography of the human retina. Arch Ophthalmol 1995;113:325–332. [PubMed: 7887846]

4. Puliafito CA, Hee MR, Lin CP, et al. Imaging of macular diseases with optical coherence tomography. Ophthalmology 1995;102:217–229. [PubMed: 7862410]

5. Hee MR, Puliafito CA, Wong C, et al. Quantitative assessment of macular edema with optical coherence tomography. Arch Ophthalmol 1995;113:1019–1029. [PubMed: 7639652]

6. Hee MR, Puliafito CA, Duker JS, et al. Topography of diabetic macular edema with optical coherence tomography. Ophthalmology 1998;105:36–70.

7. Margalit E, Sadda S. Retinal and optic nerve diseases. Artif Organs 2003;27:963–974. [PubMed: 14616515]

8. Sharma RK, Ethinger B. Management of hereditary retinal degenerations: present status and future directions. Surv Ophthalmol 1999;43:427–444. [PubMed: 10340561]

9. Ishikawa, H.; Hariprasad, R.; Wollstein, G., et al. New quality assessment parameters for OCT3. [abstract 3317/B952]; April 25-29, 2004; Fort Lauderdale, FL: The Association for Research in Vision and Ophthalmology;

10. Wojtkowski M, Bajraszewski T, Gorczynska I, et al. Ophthalmic imaging by spectral optical coherence tomography. Am J Ophthalmol 2004;138:412–419. [PubMed: 15364223]

11. Ishikawa H, Stein DM, Wollstein G, et al. Macular segmentation with optical coherence tomography. Invest Ophthalmol Vis Sci 2005;46:2012–2017. [PubMed: 15914617]

12. Anger EM, Unterhuber A, Hermann B, et al. Ultrahigh resolution optical coherence tomography of the monkey fovea. Identification of retinal sublayers by correlation with semi-thin histology sections. Exp Eye Res 2004;78:1117–1125. [PubMed: 15109918]

13. Yuodelis C, Hendrickson A. A qualitative and quantitative analysis of the human fovea during development. Vision Res 1986;26:847–855. [PubMed: 3750868]

14. Hendrickson A, Drucker D. The development of parafoveal and mid-peripheral human retina. Behav Brain Res 1992;49:21–31. [PubMed: 1388798]

15. Huang JC, Voaden MJ, Zarbin MA, Marshall J. Morphologic preservation and variability of human donor retina. Curr Eye Res 2000;20:231–241. [PubMed: 10694900]

16. Hoang QV, Linsenmeier RA, Chung CK, Curcio CA. Photoreceptor inner segments in monkey and human retina: mitochondrial density, optics, and regional variation. Vis Neurosci 2002;19:395–407. [PubMed: 12511073]

17. Gloesman M, Hermann B, Schubert C, et al. Histologic correlation of pig retina radial stratification with ultrahigh-resolution optical coherence tomography. Invest Ophthalmol Vis Sci 2003;44:1696–1703. [PubMed: 12657611]

18. Fankhauser F, Enoch J, Cibis P. Receptor orientation in retinal pathology. A first study. Am J Ophthalmol 1961;52:767–783. [PubMed: 13891537]

19. Hermann, B.; Unterhuber, A.; Wirtitsch, M., et al. Quantification of photoreceptor layer thickness using ultrahigh resolution optical coherence tomography [abstract 2373/B8]; April 25-29, 2004; Fort Lauderdale, FL: The Association for Research in Vision and Ophthalmology;

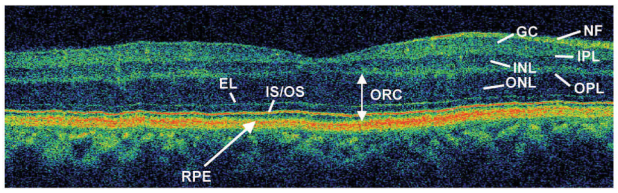

Fig 1.

Ultrahigh resolution optical coherence tomography image of a normal human macula. NFL, nerve fiber layer; GCL, ganglion cell layer; IPL, inner plexiform layer; INL, inner nuclear layer; OPL, outer plexiform layer; ONL, outer nuclear layer; ELM, external limiting membrane; IS/OS, junction between photoreceptor inner and outer segments; RPE, retinal pigment epithelium. The algorithm measures the ORC (outer retinal complex) by detecting the inner border of the RPE signal to the inner border of the ONL.

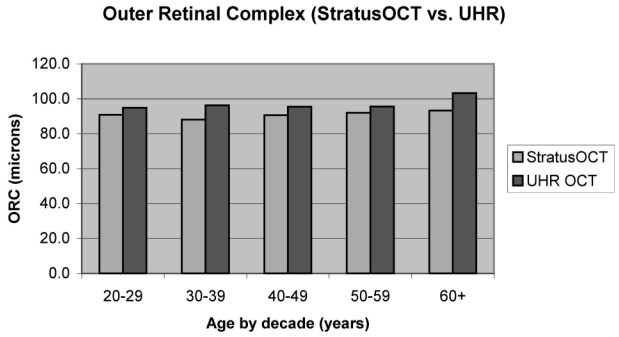

Fig 2.

Mean weighted outer retinal complex (ORC) thickness ± SD by age. Overall, the mean weighted ORC thickness ± SD was significantly lower by StratusOCT (optical coherence tomography) than by ultrahigh resolution OCT (91.1 ± 7.9 μm vs. 96.4 ± 6.3 μm, respectively; $P = 0.002$ [paired *t*-test]).